

Learning Dynamics from Infrequent Output Measurements for Uncertainty-Aware Optimal Control

Robert Lefringhausen, Theodor Springer, Sandra Hirche

*Chair of Information-oriented Control, School of Computation,
Information and Technology, Technical University of Munich, Germany
(e-mail:{robert.lefringhausen, theo.springer, hirche}@tum.de)*

Abstract: Reliable optimal control is challenging when the dynamics of a nonlinear system are unknown and only infrequent, noisy output measurements are available. This work addresses this setting of limited sensing by formulating a Bayesian prior over the continuous-time dynamics and latent state trajectory in state-space form and updating it through a targeted marginal Metropolis–Hastings sampler equipped with a numerical ODE integrator. The resulting posterior samples are used to formulate a scenario-based optimal control problem that accounts for both model and measurement uncertainty and is solved using standard nonlinear programming methods. The approach is validated in a numerical case study on glucose regulation using a Type 1 diabetes model.

Keywords: Probabilistic and Bayesian methods for system identification, Nonlinear system identification, Time series modeling, Statistical inference, Learning methods for optimal control, Model predictive control, Data-driven control theory

1. INTRODUCTION

Accurate dynamical models are fundamental for the predictive and optimal control of nonlinear systems. Although first-principles models may describe the general structure of many systems, important parameters or effects often remain unknown, limiting their direct use for control. This has sparked increasing interest in data-driven control approaches that compensate for such uncertainties by relying on data collected from the dynamical system. Yet, in many real-world applications such as robotics or biological systems, obtaining a reliable model from data is often challenging: available measurements are generally limited, only outputs may be accessible rather than full-state information, sampling may be infrequent due to hardware or communication constraints, and the data is typically corrupted by noise. Under these conditions, models learned from data carry substantial uncertainty due to limited and noisy observations, and controllers must explicitly account for this uncertainty to ensure reliable performance.

Due to these challenges, learning-based control approaches often rely on Bayesian models such as Gaussian process state-space formulations, which rigorously quantify uncertainty arising from limited data and measurement noise (Scampicchio et al., 2025). Moreover, by combining prior knowledge with available measurements, these models reduce reliance on noisy observations and provide more reliable predictions in data-sparse regimes. However, existing Bayesian approaches fall short in settings with infrequent and partial measurements. Bayesian discrete-time state-space models (Umlauft et al., 2018) require frequent full-state measurements to update the model, a requirement rarely met in practice. Continuous-time

formulations (Umlauft and Hirche, 2019) avoid the dependence on frequent measurements but require access to the full state and its time derivatives to update the prior, which is likewise infeasible in many applications. While state-estimation methods (Patwardhan et al., 2012) can reconstruct latent states and sometimes estimate selected parameters, they typically either assume known dynamics, lack principled uncertainty quantification, or rely on full-state training data, and therefore do not resolve this limitation. Bayesian time-series models (Maiworm et al., 2021) bypass the state-space representation, yet they still rely on frequent measurements and make it difficult to incorporate first-principles knowledge, which is naturally expressed in state-space form. Consequently, these approaches are not suitable for settings with infrequent, noisy output measurements, where reconstructing the latent state trajectory is essential for accurate and reliable predictions.

Recent work on uncertainty-aware control has begun to address the dependence of Bayesian state-space models on full-state measurements by placing priors over the dynamics and latent state trajectory, and jointly inferring both from output data (Lefringhausen et al., 2024, 2025). Since the resulting posterior distribution is analytically intractable, these approaches rely on Markov chain Monte Carlo (MCMC) sampling to update the model and use the resulting samples in the control design. However, existing formulations are restricted to discrete-time systems with measurements available at every time step. They therefore cannot be applied when measurements are infrequent, leaving a clear gap in uncertainty-aware optimal control when only infrequent, noisy output measurements are available.

The main contribution of this work is a novel method for uncertainty-aware optimal control of nonlinear continuous-time systems from infrequent and noisy output measurements. We formulate a prior over the continuous-time dynamics and the latent state trajectory in state-space form, enabling the incorporation of domain knowledge. To infer the posterior distribution over both the dynamics and the latent trajectory, we employ a targeted marginal Metropolis–Hastings sampler that uses a numerical ODE integrator for likelihood evaluation. Although similar ODE-based MCMC schemes have been proposed for parameter identification (Girolami, 2008), their use within a learning-based control framework has not been explored. To incorporate the inferred model and its uncertainty into the control design, we construct a scenario-based optimal control problem from the posterior samples, whose discretized form is then solved using standard numerical optimization tools. The effectiveness of the proposed approach is demonstrated in a numerical case study on glucose regulation for a Type 1 diabetes patient.

The remainder of the paper is structured as follows. Section 2 formalizes the problem setting. Section 3 introduces the marginal Metropolis–Hastings algorithm used for Bayesian inference. Section 4 presents the scenario-based optimal control formulation. Section 5 evaluates the approach in a numerical example involving a glucose–insulin dynamics model, and Section 6 concludes the paper.

2. PROBLEM FORMULATION

Consider the nonlinear continuous-time system¹

$$\dot{\mathbf{x}}(t) = \mathbf{f}_{\boldsymbol{\theta}}(\mathbf{x}(t), \mathbf{u}(t), t) \quad (1a)$$

$$\mathbf{y}(t) = \mathbf{g}_{\boldsymbol{\theta}}(\mathbf{x}(t), \mathbf{u}(t), t) + \mathbf{w}(t), \quad (1b)$$

with state $\mathbf{x}(t) \in \mathbb{R}^{n_x}$, which is not directly observed, input $\mathbf{u}(t) \in \mathbb{R}^{n_u}$, and output $\mathbf{y}(t) \in \mathbb{R}^{n_y}$. The measurements are affected by noise $\mathbf{w}(t)$, where for each fixed sampling time t_m the noise realization $\mathbf{w}(t_m)$ is drawn from a distribution $\mathcal{W}_{\boldsymbol{\theta}}(t_m)$ with density $p_{\mathcal{W}}(\mathbf{w}(t_m) \mid \boldsymbol{\theta}, t_m)$. The true dynamics function $\mathbf{f}_{\boldsymbol{\theta}}(\cdot)$, observation function $\mathbf{g}_{\boldsymbol{\theta}}(\cdot)$, and the noise distribution $\mathcal{W}_{\boldsymbol{\theta}}$ are unknown. We assume, however, that an expressive parametric model is available, and that all unknown quantities are collected in the parameter vector $\boldsymbol{\theta} \in \mathbb{R}^{n_{\boldsymbol{\theta}}}$. Such parameterizations naturally arise in systems governed by physical laws, which often dictate the structure of the dynamics or measurement process, thereby enabling informative and interpretable models.

At the current time $t = 0$, we assume access to historical measurements of the system. Negative times $t \in [-T, 0]$ refer to this past data window, whereas positive times $t > 0$ correspond to the control horizon. Within the training window $[-T, 0]$, the input trajectory $\mathbf{u}(t)$ is known, and

¹ **Notation:** Lower/upper case bold symbols denote vectors/matrices, respectively. \mathbb{R} denotes the set of real numbers, \mathbb{Z} the set of integers, \mathbb{N}^0 and \mathbb{N} the set of natural numbers with and without zero, and subscripts $<_a$ or \leq_a the corresponding subsets whose elements satisfy $< a$ or $\leq a$. The notation $\mathbf{a}_{b:c}$ is shorthand for $\{\mathbf{a}_b, \dots, \mathbf{a}_c\}$. (Multivariate) Gaussian distributed random variables with mean $\boldsymbol{\mu}$ and variance $\boldsymbol{\Sigma}$ are denoted by $\mathcal{N}(\boldsymbol{\mu}, \boldsymbol{\Sigma})$. \mathbf{I}_n denotes the $n \times n$ identity matrix and $\mathbf{0}$ the zero matrix of appropriate dimension.

M output measurements $\mathbf{y}_m = \mathbf{y}(t_m)$ are available at a (possibly irregular) set of sampling instants $t_{1:M} \subseteq [-T, 0]$. This yields the dataset

$$\mathbb{D} = \{\mathbf{u}(t) \text{ for } t \in [-T, 0], \mathbf{y}_{1:M}\}, \quad (2)$$

which contains the complete input trajectory and the corresponding noisy output measurements.

To enable Bayesian inference of both the dynamics and the latent state trajectory, we make the following standard assumption.

Assumption 1. Priors $p(\boldsymbol{\theta})$ and $p(\mathbf{x}(-T))$ are available for the model parameters and for the initial state at the beginning of the training window. The unknown parameters and initial state are drawn from these priors.

This assumption is natural in many practical settings: domain knowledge, operational limits, or previous experiments often provide informative priors for the model parameters and for the range of feasible initial states.

The objective is to find an input trajectory $\mathbf{u}(t)$ over a finite prediction horizon $[0, H]$ that minimizes the continuous-time cost functional

$$J(\mathbf{u}(\cdot), \mathbf{x}(\cdot)) = c_t(\mathbf{x}(H)) + \int_0^H c(\mathbf{u}(t), \mathbf{x}(t), t) dt, \quad (3)$$

where c denotes the running cost and c_t denotes the terminal cost. The input trajectory $\mathbf{u}(\cdot)$ must be chosen so that the resulting trajectory satisfies the constraints

$$\mathbf{h}(\mathbf{u}(t), \mathbf{x}(t), t) \leq \mathbf{0} \quad \forall t \in [0, H]. \quad (4)$$

This problem represents the ideal formulation, which would be solvable only under perfect knowledge of the system and its initial state. However, because the system evolution must be inferred from limited data, constraint satisfaction cannot be guaranteed deterministically. The objective is therefore to compute input trajectories that explicitly account for model uncertainty, yielding solutions that are expected to remain feasible and to achieve low cost under likely realizations of the system’s evolution.

To address this problem, we first infer a posterior distribution over the unknown dynamics and latent state trajectory using a targeted marginal Metropolis–Hastings scheme equipped with a numerical integrator. Posterior samples obtained in this way represent plausible system evolutions consistent with the available data and prior knowledge. These samples are then used to construct a discretized scenario-based approximation of the optimal control problem (3–4), from which a robust input trajectory is computed.

3. MARGINAL METROPOLIS–HASTINGS SAMPLING

A central step in the proposed framework is the inference of the posterior distribution $p(\boldsymbol{\theta}, \mathbf{x}(0) \mid \mathbb{D})$, which combines prior information about the unknown model parameters with evidence from the infrequently sampled and noisy measurements, thereby reducing the potentially large model uncertainty that would arise if one relied on the prior alone. We specifically target the state $\mathbf{x}(0)$ because, due to the Markov property inherent in the state-space representation (1), $\mathbf{x}(0)$ summarizes all information that is relevant for predicting the system’s future evolution

($t > 0$). In accordance with Bayes' theorem, this posterior distribution is proportional to the product of the prior distribution and the likelihood function. Because the state trajectory $\mathbf{x}(t)$ is unobserved and evolves in continuous time, evaluating the likelihood requires marginalizing over all admissible latent trajectories, which leads to an analytically intractable integral (Andrieu et al., 2010). To address this difficulty, we employ a targeted marginal Metropolis–Hastings (MMH) scheme equipped with a numerical ODE integrator to draw samples from the joint posterior over parameters and latent states. This section introduces the sampling-based inference procedure used to obtain these posterior samples.

The key idea of MMH sampling (Robert and Casella, 2004) is to generate proposals for the uncertain quantities and accept or reject them based on how well they explain the available measurements. Since the latent state trajectory of a continuous-time system is uniquely determined by the parameters and the initial state, the sampler proposes only a pair $\mathbf{z} = (\boldsymbol{\theta}, \mathbf{x}(-T))$ rather than a full trajectory. Proposals are drawn from a distribution $q(\mathbf{z}' | \mathbf{z}^{[k]})$ whose support covers the priors $p(\boldsymbol{\theta})$ and $p(\mathbf{x}(-T))$, and are accepted or rejected using the Metropolis–Hastings criterion. The complete MMH procedure is summarized in Algorithm 1.

Evaluating the acceptance probability requires computing the likelihood of the measurement sequence under a proposed pair \mathbf{z}' , i.e., $p(\mathbf{y}_{1:M} | \mathbf{z}')$. This, in turn, requires propagating the latent state trajectory between the measurement instants $t_{1:M}$. Let

$$\mathbf{x}(t_m)' = \Phi(t_m; \mathbf{z}', \mathbf{u}(\cdot)) \quad (5)$$

denote the solution of the ODE (1) at time t_m , obtained by integrating the dynamics forward from the initial state $\mathbf{x}'(-T)$ under parameters $\boldsymbol{\theta}'$ and the known input trajectory $\mathbf{u}(\cdot)$, where Φ denotes the associated flow map. Since Φ is not available in closed form, it is approximated numerically. Let

$$\hat{\mathbf{x}}(t_m)' \approx \Phi(t_m; \mathbf{z}', \mathbf{u}(\cdot)) \quad (6)$$

denote the numerical approximation returned by the ODE solver. For each measurement instant, we define the residual

$$\mathbf{r}_m(\mathbf{z}') := \mathbf{y}_m - \mathbf{g}_{\boldsymbol{\theta}'}(\hat{\mathbf{x}}(t_m)', \mathbf{u}(t_m), t_m). \quad (7)$$

The likelihood of the observed output measurements is then computed as

$$p(\mathbf{y}_{1:M} | \mathbf{z}', \mathbf{u}(\cdot)) \approx \prod_{m=1}^M p_{\mathcal{W}}(\mathbf{r}_m(\mathbf{z}') | \boldsymbol{\theta}', t_m). \quad (8)$$

The acceptance probability for a proposed pair \mathbf{z}' is given by the standard Metropolis–Hastings ratio (Robert and Casella, 2004)

$$\alpha = \min \left(1, \frac{p(\mathbf{y}_{1:M} | \mathbf{z}') p(\mathbf{z}') q(\mathbf{z}^{[k]} | \mathbf{z}')}{p(\mathbf{y}_{1:M} | \mathbf{z}^{[k]}) p(\mathbf{z}^{[k]}) q(\mathbf{z}' | \mathbf{z}^{[k]})} \right). \quad (9)$$

This ratio compares the posterior plausibility of the proposed and current pair, weighted by the proposal densities. Proposals that better explain the observed data are more likely to be accepted. If a proposal is accepted, it becomes the next state of the Markov chain; otherwise, the chain remains at its current state. Finally, the sampled posterior $p(\boldsymbol{\theta}, \mathbf{x}(-T) | \mathbb{D})$ is mapped to the target posterior $p(\boldsymbol{\theta}, \mathbf{x}(0) | \mathbb{D})$ by propagating the initial state forward to

Algorithm 1 Marginal Metropolis–Hastings sampler

Input: Observations \mathbb{D} , model $\mathbf{f}_{\boldsymbol{\theta}}(\cdot)$, $\mathbf{g}_{\boldsymbol{\theta}}(\cdot)$, $p_{\mathcal{W}}(\cdot | \boldsymbol{\theta})$, priors $p(\boldsymbol{\theta})$, $p(\mathbf{x}(-T))$, proposal density $q(\mathbf{z}' | \mathbf{z})$, initial value $\mathbf{z}^{[1]}$, number of samples K , burn-in period K_b , thinning parameter k_d

Output: K samples from $p(\boldsymbol{\theta}, \mathbf{x}(0) | \mathbb{D})$

- 1: Initialize: $k \leftarrow 1$
 - 2: Compute likelihood $p(\mathbf{y}_{1:M} | \mathbf{z}^{[1]})$ using (8)
 - 3: **while** $k \leq K_b + 1 + (K - 1)(k_d + 1)$ **do**
 - 4: Propose $\mathbf{z}' \sim q(\mathbf{z}' | \mathbf{z}^{[k]})$
 - 5: Simulate latent trajectory under \mathbf{z}' and evaluate $p(\mathbf{y}_{1:M} | \mathbf{z}')$ using (8)
 - 6: Compute acceptance probability α using (9)
 - 7: **if** $\text{Uniform}(0, 1) < \alpha$ **then**
 - 8: Accept proposal: $k \leftarrow k + 1$, $\mathbf{z}^{[k]} \leftarrow \mathbf{z}'$
 - 9: **end if**
 - 10: **end while**
 - 11: Discard burn-in and perform thinning
 - 12: Compute $\mathbf{x}^{[k]}(0) = \Phi(0; \mathbf{z}^{[k]})$ for each retained sample
-

time $t = 0$ using the ODE flow map, which is again approximated using the same numerical integrator employed during likelihood evaluation.

Under mild regularity assumptions on the dynamics and the proposal distribution, the MMH kernel defined using the exact flow map Φ admits the desired posterior $p(\mathbf{z} | \mathbb{D})$ as its invariant distribution (Tierney, 1994). In other words, if the latent trajectory were propagated using the exact solution of the ODE, the resulting Markov chain would converge asymptotically to the true posterior, ensuring that the obtained samples are correctly distributed. In practice, however, the flow map Φ is not available in closed form and must be approximated numerically. When the likelihood is evaluated using numerically propagated states $\hat{\mathbf{x}}(t_m)$ instead of the exact trajectory $\Phi(t_m; \mathbf{z})$, the resulting Metropolis–Hastings transition kernel becomes an approximation of the ideal one. This introduces a small bias in the stationary distribution. Nevertheless, the integration error is typically negligible compared with the intrinsic stochastic variability of the sampler, so the approximate chain remains a high-quality surrogate of the exact posterior.

Remark 1. Efficient MMH sampling relies critically on a proposal distribution that is well aligned with the geometry of the posterior. In the present setting, the parameters and the initial state jointly determine the latent trajectory used to explain the measurements, which induces strong correlations in their posterior. A proposal that does not reflect this structure typically leads to poor mixing, low acceptance rates, and highly autocorrelated samples (Lefringhausen et al., 2025). A practical approach to constructing an effective proposal is staged inference, where the sampler initially uses only a subset of the measurements and gradually increases the number of data points used in the likelihood evaluation. At each stage, the proposal covariance can be adapted based on the empirical covariance of the chain, allowing the proposal to track the evolving posterior geometry and account for the induced parameter–state correlations.

After running the MMH sampler, the raw sequence of generated samples does not yet constitute a representative

set from the target posterior. The first samples of the chain depend heavily on the (generally arbitrary) initialization and may not represent the target distribution. To mitigate this effect, the initial K_b samples are discarded, which is commonly referred to as the burn-in period. In addition, consecutive samples of the MMH sampler are typically correlated, since each new proposal is generated conditionally on the previous accepted sample. For the intended use, strongly autocorrelated samples are undesirable, as they may underrepresent the variability of the posterior distribution. To reduce this autocorrelation, we apply thinning: out of every block of $k_d + 1$ samples, only one sample is retained, while the remaining k_d samples are discarded. The thinning parameter k_d must be chosen to balance statistical independence and computational efficiency—large enough to ensure that the retained samples exhibit acceptably low autocorrelation, but not so large that an excessive number of samples is discarded. The resulting thinned sequence constitutes a set of samples that are approximately independent draws from the target posterior $p(\boldsymbol{\theta}, \mathbf{x}(0) \mid \mathbb{D})$. These posterior samples represent plausible realizations of the system dynamics consistent with the available data and prior knowledge and form the basis for the scenario-based optimal control formulation described in the next section.

4. SCENARIO-BASED OPTIMAL CONTROL

In this section, we describe how the posterior samples obtained from the MMH sampler in Section 3 can be used to compute an input trajectory that is robust to likely realizations of the actual system dynamics. Section 4.1 introduces the underlying idea and formulates the scenario-based optimal control problem in continuous time, while Section 4.2 presents its numerical discretization and solution using standard nonlinear programming techniques.

4.1 Scenario-Based Optimal Control in Continuous Time

The central idea of the proposed approach is to design a control input that remains feasible and performs well across the range of system behaviors that are plausible under the learned posterior distribution. Rather than relying on a single nominal model or adopting overly conservative worst-case assumptions, we directly exploit the posterior samples $\{\boldsymbol{\theta}, \mathbf{x}(0)\}^{[1:K]}$ generated by the MMH sampler. Each such sample specifies one plausible realization of the model parameters and current state, consistent with the available measurements and prior information. Because the state evolution of a continuous-time system is uniquely determined by its parameters, initial condition, and input trajectory, each posterior sample induces a distinct possible future trajectory. We therefore interpret these samples as scenarios.

In the proposed scenario-based optimal control formulation, all scenarios are propagated forward under a shared control input trajectory. State and input constraints are enforced for every scenario, while the overall objective aggregates the individual scenario costs. This construction yields a control law that is explicitly robustified against the posterior uncertainty.

Under a candidate control trajectory $\mathbf{u}(\cdot)$, each scenario evolves according to the ODE flow map

$$\mathbf{x}^{[k]}(t) = \Phi\left(t; \boldsymbol{\theta}^{[k]}, \mathbf{x}^{[k]}(0), \mathbf{u}(\cdot)\right), \quad t \in [0, H]. \quad (10)$$

Replacing the unknown true trajectory in (3–4) with the scenario trajectories yields a scenario-based version of the optimal control problem. In this formulation, the cost is approximated by the empirical average over the K posterior samples, and all constraints are enforced for every scenario. This yields the following scenario-averaged cost functional

$$J_{\text{sc}}(\mathbf{u}(\cdot)) := \frac{1}{K} \sum_{k=1}^K \left[c_f(\mathbf{x}^{[k]}(H)) + \int_0^H c(\mathbf{u}(t), \mathbf{x}^{[k]}(t), t) dt \right], \quad (11)$$

and the continuous-time scenario optimal control problem becomes

$$\min_{\mathbf{u}(\cdot)} J_{\text{sc}}(\mathbf{u}(\cdot)) \quad (12a)$$

$$\text{s.t. } \forall t \in [0, H], \quad \forall k \in \mathbb{N}_{\leq K},$$

$$\mathbf{x}^{[k]}(t) = \Phi\left(t; \boldsymbol{\theta}^{[k]}, \mathbf{x}^{[k]}(0), \mathbf{u}(\cdot)\right), \quad (12b)$$

$$\mathbf{h}(\mathbf{u}(t), \mathbf{x}^{[k]}(t), t) \leq \mathbf{0}. \quad (12c)$$

By construction, this formulation discourages control inputs that lead to constraint violations or poor performance across the posterior samples, thereby yielding input trajectories that are robust with respect to the uncertainty captured by these scenarios.

4.2 Time Discretization and Numerical Implementation

Since the scenario-based optimal control problem (12) is posed in continuous time, it cannot be solved directly with standard numerical optimization methods. We therefore introduce a time discretization of the dynamics, costs, and constraints, which yields a finite-dimensional nonlinear program suitable for numerical solution. Following the direct multiple-shooting framework (Betts, 2010), we introduce a control grid

$$0 = \tau_0 < \tau_1 < \dots < \tau_N = H, \quad (13)$$

and restrict the control input to be piecewise constant over each interval,

$$\mathbf{u}(t) = \mathbf{u}_n, \quad t \in [\tau_n, \tau_{n+1}), \quad \forall n \in \mathbb{N}_{\leq N}^0, \quad (14)$$

so that the collection $\mathbf{u}_{0:N-1}$ constitutes the decision variables of the discretized problem.

For each scenario $k = 1, \dots, K$, the continuous-time dynamics are discretized by numerically propagating the ODE (1) over each interval $[\tau_n, \tau_{n+1})$ using the sampled parameters $\boldsymbol{\theta}^{[k]}$ and initial state $\mathbf{x}^{[k]}(0)$. Let

$$\mathbf{x}_{n+1}^{[k]} = \Psi\left(\tau_{n+1}, \tau_n; \mathbf{x}_n^{[k]}, \mathbf{u}_n, \boldsymbol{\theta}^{[k]}\right), \quad \forall n \in \mathbb{N}_{\leq N}^0, \quad (15)$$

denote the numerical flow map produced by the ODE integrator, with $\mathbf{x}_0^{[k]} = \mathbf{x}^{[k]}(0)$. The map Ψ is the discrete counterpart of the continuous-time flow Φ and is computed using the same numerical solver used during the MMH inference step.

The continuous-time cost functional is approximated by

$$\hat{J}_{\text{sc}} = \frac{1}{K} \sum_{k=1}^K \left[c_f(\mathbf{x}_N^{[k]}) + \sum_{n=0}^{N-1} c(\mathbf{u}_n, \mathbf{x}_n^{[k]}, \tau_n) \Delta_n \right], \quad (16)$$

where $\Delta_n = \tau_{n+1} - \tau_n$ denotes the grid spacing.

The constraints (4) are imposed at all grid points for every scenario, i.e.,

$$\mathbf{h}(\mathbf{u}_n, \mathbf{x}_n^{[k]}, \tau_n) \leq \mathbf{0}, \quad \forall n \in \mathbb{N}_{\leq N}^0, \quad \forall k \in \mathbb{N}_{\leq K}. \quad (17)$$

The discretized scenario-based optimal control problem then becomes the nonlinear program

$$\min_{\mathbf{u}_{0:N-1}} \hat{J}_{\text{sc}}, \quad (18a)$$

$$\text{s.t.} \quad \forall n \in \mathbb{N}_{\leq N}^0, \quad \forall k \in \mathbb{N}_{\leq K}, \quad \mathbf{x}_{n+1}^{[k]} = \Psi(\tau_{n+1}, \tau_n; \mathbf{x}_n^{[k]}, \mathbf{u}_n, \boldsymbol{\theta}^{[k]}), \quad (18b)$$

$$\mathbf{h}(\mathbf{u}_n, \mathbf{x}_n^{[k]}, \tau_n) \leq \mathbf{0}. \quad (18c)$$

The resulting finite-dimensional optimization problem can be solved using standard nonlinear programming solvers; see (Nocedal and Wright, 2006).

The robustness of the resulting control law depends on several interacting factors. First, since the constraints in (18) are imposed only at the discretization nodes $\tau_{0:N}$, they ensure feasibility only at these time points. Even with a perfect model, constraint satisfaction between nodes cannot be guaranteed merely by pointwise enforcement; refining the grid reduces the risk of inter-sample violations but increases the computational burden of the NLP (Betts, 2010). Second, the extent to which the scenario program captures the underlying uncertainty is governed by both the number and the diversity of the posterior samples. Increasing the number of approximately independent samples generally improves robustness, as it provides a broader and more representative coverage of the posterior distribution, thereby exposing the optimizer to a wider range of plausible system behaviors. Conversely, strong autocorrelation in the Markov chain leads to clusters of nearly identical scenarios, artificially narrowing the represented uncertainty and weakening the practical robustness of the computed input trajectory. Finally, the predicted state trajectories rely on numerical integration of the dynamics. For consistency between learning and control, it is advisable to employ the same ODE solver used during posterior inference. Although numerical integration introduces an additional approximation error, this effect is typically less significant than the uncertainty encoded in the posterior samples and the discretization error associated with the finite control grid.

It is worth noting that, under the idealized assumption of perfect numerical integration, one could formalize this robustness and provide probabilistic guarantees of constraint satisfaction at the grid points. Such guarantees may be obtained by validating the computed input trajectory on an additional set of posterior samples or, alternatively, by adopting a robust cost formulation and invoking results from robust optimization; closely related arguments have been established in (Lefringhausen et al., 2024). However, this lies beyond the scope of the present work. Instead, the practical robustness of the proposed approach is demonstrated in the numerical case study of the following section.

5. SIMULATION

This section evaluates the proposed Bayesian inference and control framework in a numerical case study of glucose

regulation in Type 1 diabetes. This setting provides a natural test case for the proposed method: the dynamics are nonlinear and patient-specific, only the glucose level is directly measurable, and measurements typically occur at irregular sampling times. At the same time, glucose regulation is a safety-critical task: inadequate control actions can induce hypo- or hyperglycemia, both of which carry significant medical risks. These characteristics make this setting well-suited for evaluating the proposed framework, which infers parameters and latent states from infrequent measurements, quantifies the associated uncertainty, and uses this information to compute control inputs that remain robust under the inferred uncertainty.

5.1 Setup

For the simulation², we employ a version of the Bergman minimal model (Bergman et al., 1981), which is extended with meal disturbances and exogenous insulin infusion, as in (Ali and Padhi, 2011). The model captures the interaction between blood glucose $G(t)$ [mg/dL], plasma insulin $I(t)$ [mU/L], and a remote insulin action state $X(t)$ [1/min] that represents the delayed effect of insulin on glucose uptake. The continuous-time dynamics are given by

$$\dot{G}(t) = -p_1 (G(t) - G_b) - X(t)G(t) + D(t), \quad (19a)$$

$$\dot{X}(t) = -p_2 X(t) + p_3 (I(t) - I_b), \quad (19b)$$

$$\dot{I}(t) = -n (I(t) - I_b) + u(t), \quad (19c)$$

where t denotes time (in minutes), the parameters p_1 , p_2 , and p_3 characterize insulin action dynamics, n is the insulin clearance rate, and G_b and I_b denote basal levels. The input $u(t)$ represents exogenous insulin infusion delivered by an insulin pump, while $D(t)$ denotes glucose appearance resulting from meals and is assumed to be known in this study. For Type 1 diabetes patients, the glucose effectiveness parameter p_1 is physiologically negligible and therefore omitted in our simulations, resulting in $\dot{G}(t) = -X(t)G(t) + D(t)$ (Ali and Padhi, 2011).

We simulate the system over an 18-hour period (6 am–12 am). Meal disturbances are modeled using the exponential appearance profile

$$D(t) = S_{\text{meal}} B e^{-B(t-t_{\text{meal}})}, \quad t \geq t_{\text{meal}}, \quad (20)$$

where S_{meal} denotes the meal size, t_{meal} is the meal time, and $B = 0.5 \text{ min}^{-1}$ controls the decay rate. Three meals are administered at 8 am ($S_{\text{meal}} = 60 \text{ mg/dL}$), 1 pm ($S_{\text{meal}} = 90 \text{ mg/dL}$), and 7 pm ($S_{\text{meal}} = 80 \text{ mg/dL}$).

The first part of the simulation (6 am–6 pm), which includes the meals at 8 am and 1 pm, is used as training data for Bayesian inference. The remaining segment (6 pm–12 am), containing the 7 pm meal, is used to evaluate the control strategy. To keep the simulated trajectory physiologically plausible, we model a simple insulin dose as the input signal $u(t)$ during the training period: each meal triggers an amount of insulin proportional to the meal size, delivered over a one-hour window.

In practice, glucose measurements can occur at infrequent and irregular time points due to sensor limitations and intermittent reporting. To mimic this setting, we sample

² The code is available at github.com/TUM-ITR/ode-mmh-planner

Table 1. Priors and nominal values used in the simulation study.

Parameter	Prior distribution	Nominal value
p_2	$\text{LogNormal}(-4.26, 0.18^2)$	0.63
p_3	$\text{LogNormal}(-13.27, 0.28^2)$	1.12
n	$\text{LogNormal}(-1.66, 0.23^2)$	0.22
$G(-T)$	$\mathcal{N}(80.0, 8.0^2)$	80.0
$X(-T)$	$\mathcal{N}(0.0, 0.001^2)$	0.0
$I(-T)$	$\mathcal{N}(7.0, 2.0^2)$	7.0

$M = 200$ measurement instants uniformly from the training window. The corresponding glucose measurements are corrupted by zero-mean Gaussian noise

$$y_m = G(t_m) + v_m, \quad v_m \sim \mathcal{N}(0, \sigma^2), \quad (21)$$

with standard deviation $\sigma = 8 \text{ mg/dL}$. The remaining states $X(t)$ and $I(t)$ are unmeasured and thus remain latent.

The control objective is to maintain the glucose concentration close to a target level of $G_{\text{ref}} = 80 \text{ mg/dL}$ while compensating for meal-induced disturbances and respecting physiological safety constraints. The continuous-time cost functional over a prediction horizon of $H = 6$ hours is

$$J = W_{G_f} (G(H) - G_{\text{ref}})^2 + \int_0^H \left(W_G (G(t) - G_{\text{ref}})^2 + W_U u(t)^2 \right) dt, \quad (22)$$

with weights $W_G = 1$, $W_{G_f} = 10$, and $W_U = 10^{-4}$, so that the objective is dominated by glucose regulation while the regularization term discourages unnecessarily aggressive insulin delivery. To reduce the risk of hypo- and hyperglycemia and thus ensure patient safety, we enforce the clinically recommended bounds $70 \text{ mg/dL} \leq G(t) \leq 180 \text{ mg/dL}$. In addition, the insulin infusion rate is constrained by $0 \leq u(t) \leq 20 \text{ mU/min}$, reflecting typical limits of commercial insulin pumps.

A key advantage of the proposed method is that the prior is formulated directly in state-space form. Since physiological knowledge about glucose–insulin regulation is typically available in this representation, models such as the Bergman minimal model can be incorporated naturally, and only the model parameters must be inferred from data. For the parameter estimation, we assume the basal insulin level is known and fix it at $I_b = 7 \text{ mU/L}$ (Ali and Padhi, 2011), which is also used in the simulated ground-truth dynamics. We then estimate the parameters p_2 , p_3 , and n together with the latent state trajectory. To ensure positivity and reflect prior uncertainty around physiologically plausible values, we place independent lognormal priors on p_2 , p_3 , and n . The initial state at 6 am is modeled as Gaussian and centered at physiologically plausible fasting levels: glucose around 80 mg/dL and insulin near its basal concentration I_b . The exact prior distributions are summarized in Table 1.

To improve mixing of the MMH sampler, we employ the adaptive proposal strategy described in Remark 1. For numerically integrating the dynamics in the MMH sampler (Algorithm 1) and for discretizing the optimal control problem, we use a fourth-order Runge–Kutta scheme with

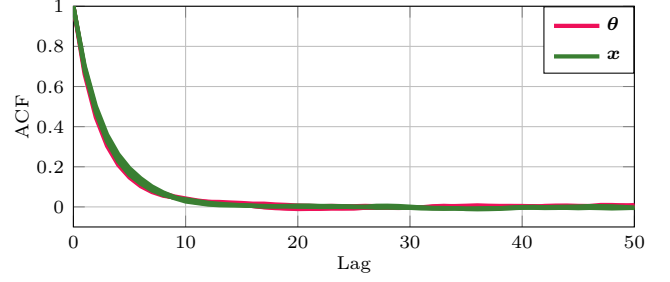


Fig. 1. Normalized autocorrelation functions (ACFs) of successive samples generated by the MMH sampler without thinning. Red curves show the ACFs of the model parameters (p_2, p_3, n), and green curves show the ACFs of the initial state components $\mathbf{x}(-T)$ at the start of the training window.

a step size of 0.5 min . The ground-truth trajectory is simulated using the Tsitouras 5/4 method (Tsitouras, 2011).

5.2 Results

We begin by assessing the autocorrelation structure of the samples produced by the MMH sampler (Algorithm 1) in order to determine an appropriate thinning interval. To this end, we draw one representative parameter realization from the prior, generate the corresponding measurements, and run the MMH sampler for $K = 10^5$ iterations without thinning. We then compute the normalized autocorrelation functions (ACFs) of the model parameters θ and the initial state $\mathbf{x}(-T)$. As shown in Figure 1, the autocorrelation of all components decays substantially within a lag of 25. Based on this observation, we apply a thinning factor of $k_d = 25$ in all subsequent experiments to obtain approximately independent samples.

To assess the robustness of the proposed method with respect to variability in patient dynamics and initial conditions, we conduct a Monte Carlo study consisting of 100 independent simulation runs. In each run, the true physiological parameters p_2 , p_3 , and n , as well as the initial state at 6 am, are sampled from the prior distributions given in Table 1. For each sampled instance, measurements are generated over the training window, and the MMH sampler is used to obtain $K = 100$ posterior samples. These samples are then used to formulate the optimal control problem described in Section 4, which is solved using JuMP (Lubin et al., 2023), IPOPT (Wächter and Biegler, 2006), and the HSL linear solvers (HSL, 2025). The resulting control input is then applied to the corresponding true system realization to evaluate the system response.

For comparison, we also evaluate a nominal-model baseline. In this approach, the parameters are fixed at the nominal values listed in Table 1, and the latent state is estimated using an extended Kalman filter (EKF) equipped with the same RK4 integration scheme to accommodate infrequent measurements. The optimal input trajectory is then computed using this nominal model and the EKF state estimate as the initial condition.

Table 2 shows that the nominal-model EKF baseline violates the prescribed glucose safety bounds of 70–

Table 2. Cost and constraint violations over 100 Monte Carlo runs.

Method	Cost ($\times 10^4$)	Violations
MMH-scenario	8.98 ± 3.50	0/100
Nominal + EKF	16.54 ± 13.27	44/100

180 mg/dL in 44 of the 100 runs, highlighting its inability to maintain physiologically safe glucose levels under uncertainty. In contrast, the proposed MMH-scenario approach satisfies all constraints in every run, demonstrating strong robustness to uncertainty in both the model parameters and the latent state. The proposed method also achieves substantially lower costs. By jointly inferring the state and the model parameters and optimizing over multiple posterior scenarios, it obtains more accurate and reliable predictions than a single nominal model, resulting in more effective control actions and improved overall performance.

Figure 2 shows the glucose predictions of the MMH-scenario method together with the realized trajectory for one representative run. The meal at 7 pm (corresponding to $t = 60$ min in the control horizon) induces a rise in glucose. Because the controller knows the timing and magnitude of this disturbance, it increases insulin delivery in anticipation of the meal, causing glucose to decrease slightly beforehand and thereby reducing the magnitude of the subsequent spike. After the meal, the glucose concentration returns toward the target level of 80 mg/dL. Throughout the entire horizon, the realized trajectory remains within the prescribed safety bounds of 70–180 mg/dL and stays inside the envelope of the sampled scenarios, indicating that the scenario-based predictions provide a reliable foundation for control.

In contrast, the Nominal + EKF baseline produces substantially less accurate predictions and consequently violates the safety constraints. Toward the end of the horizon, the glucose level falls to approximately 60 mg/dL, entering a hypoglycemic range. This example highlights the risks associated with nominal-model strategies in safety-critical settings, where reliable uncertainty quantification is crucial for ensuring safe operation.

Overall, the results demonstrate that the MMH-scenario method provides reliable and safe control performance across a wide range of physiologically plausible patient models.

6. CONCLUSION

This paper presents a method for uncertainty-aware optimal control of nonlinear continuous-time systems from infrequent and noisy output measurements. A prior over the dynamics in state-space representation is updated using a marginal Metropolis–Hastings sampler, and the resulting samples are used to formulate a scenario optimal control problem. A numerical case study on glucose regulation demonstrates the effectiveness and robustness of the approach.

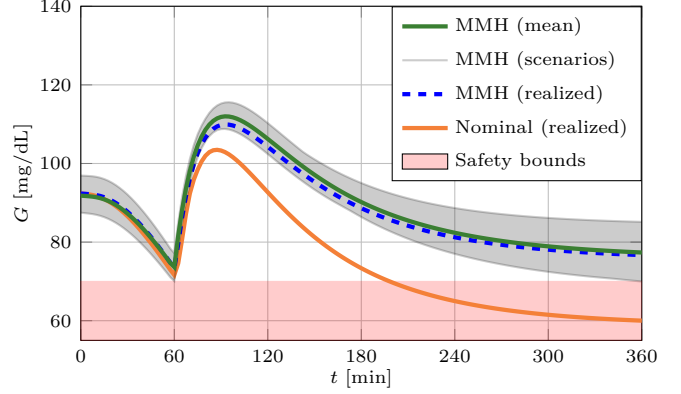


Fig. 2. Glucose trajectories over the control horizon for one representative run. The green curve shows the mean prediction of the MMH-scenario planner, and the gray band denotes the envelope of the 100 posterior scenarios used for planning. The dashed blue curve depicts the realized trajectory obtained when applying the MMH-scenario control input, while the solid orange curve shows the realized trajectory under the Nominal + EKF baseline. The red bands indicate the prescribed safety bounds.

DECLARATION OF GENERATIVE AI AND AI-ASSISTED TECHNOLOGIES IN THE WRITING PROCESS

During the preparation of this work, the authors utilized Grammarly and ChatGPT to enhance language and readability, as well as ChatGPT and GitHub Copilot to aid in programming the simulation. After using these tools, the authors reviewed and edited the content as needed and take full responsibility for the content of the publication.

REFERENCES

- Ali, S.F. and Padhi, R. (2011). Optimal blood glucose regulation of diabetic patients using single network adaptive critics. *Optimal Control Applications and Methods*, 32(2), 196–214.
- Andrieu, C., Doucet, A., and Holenstein, R. (2010). Particle Markov chain Monte Carlo methods. *Journal of the Royal Statistical Society Series B: Statistical Methodology*, 72(3), 269–342.
- Bergman, R.N., Phillips, L.S., Cobelli, C., et al. (1981). Physiologic evaluation of factors controlling glucose tolerance in man: measurement of insulin sensitivity and beta-cell glucose sensitivity from the response to intravenous glucose. *The Journal of clinical investigation*, 68(6), 1456–1467.
- Betts, J.T. (2010). *Practical methods for optimal control and estimation using nonlinear programming*. SIAM.
- Girolami, M. (2008). Bayesian inference for differential equations. *Theoretical Computer Science*, 408(1), 4–16.
- HSL (2025). A collection of Fortran codes for large scale scientific computation. <http://www.hsl.rl.ac.uk/>.
- Lefringhausen, R., Noel Aziz Hanna, S.L., August, E., and Hirche, S. (2025). Barrier certificates for unknown systems with latent states and polynomial dynamics using Bayesian inference. *arXiv preprint arXiv:2504.01807*.

- Lefringhausen, R., Srithasan, S., Lederer, A., and Hirche, S. (2024). Learning-based optimal control with performance guarantees for unknown systems with latent states. In *2024 European Control Conference (ECC)*, 90–97.
- Lubin, M., Dowson, O., Dias Garcia, J., Huchette, J., Legat, B., and Vielma, J.P. (2023). JuMP 1.0: Recent improvements to a modeling language for mathematical optimization. *Mathematical Programming Computation*, 15(3), 581–589.
- Maiworm, M., Limon, D., and Findeisen, R. (2021). Online learning-based model predictive control with Gaussian process models and stability guarantees. *International Journal of Robust and Nonlinear Control*, 31(18), 8785–8812.
- Nocedal, J. and Wright, S.J. (2006). *Numerical optimization*. Springer, New York, NY, USA, 2. edition.
- Patwardhan, S.C., Narasimhan, S., Jagadeesan, P., Gopaluni, B., and Shah, S.L. (2012). Nonlinear Bayesian state estimation: A review of recent developments. *Control Engineering Practice*, 20(10), 933–953.
- Robert, C.P. and Casella, G. (2004). *Monte Carlo statistical methods*, volume 2. Springer.
- Scampicchio, A., Arcari, E., Lahr, A., and Zeilinger, M.N. (2025). Gaussian processes for dynamics learning in model predictive control. *Annual Reviews in Control*, 60, 101034.
- Tierney, L. (1994). Markov chains for exploring posterior distributions. *The Annals of Statistics*, 1701–1728.
- Tsitouras, C. (2011). Runge–Kutta pairs of order 5 (4) satisfying only the first column simplifying assumption. *Computers & mathematics with applications*, 62(2), 770–775.
- Umlauft, J., Beckers, T., and Hirche, S. (2018). Scenario-based optimal control for Gaussian process state space models. In *2018 European Control Conference (ECC)*, 1386–1392. IEEE.
- Umlauft, J. and Hirche, S. (2019). Feedback linearization based on Gaussian processes with event-triggered online learning. *IEEE Transactions on Automatic Control*, 65(10), 4154–4169.
- Wächter, A. and Biegler, L.T. (2006). On the implementation of an interior-point filter line-search algorithm for large-scale nonlinear programming. *Mathematical programming*, 106, 25–57.